

Characterization and tunneling conductance spectra of N,N'-bis(9H-fluoren-9-ylidene)benzene-1,4-diamine thin films on graphite

Hongliang Xin, Zhuomin Li, Tianxian He, Xinrui Miao, Wenli Deng*

College of Materials Science and Engineering, South China University of Technology, Guangzhou 510640, China

ARTICLE INFO

Article history:

Received 21 October 2009

Received in revised form 20 January 2010

Accepted 19 February 2010

Keywords:

Thin films

Organic compounds

Electrical properties

Electrical characterization

ABSTRACT

N,N'-bis(9H-fluoren-9-ylidene)benzene-1,4-diamine was synthesized via the acetic acid-assisted Schiff base reaction between 9-fluorenone and p-phenylenediamine. The thin films were deposited from solution and characterized by contact angle measurements (CAM), X-ray photoelectron spectroscopy (XPS) and tunneling conductance spectroscopy (TCS). The tunneling conductance spectra, related to the potential and distance between the tip and substrate, were acquired at different tip–substrate separations and depicted significant trend under the action of electric field. Systematic analysis shows more information about electron transport through medium layers. The electric field plays an important role in tunneling conductance spectra. The tunneling conductance spectra data indicate the electric field dependence of electron transport.

© 2010 Elsevier B.V. All rights reserved.

1. Introduction

The π conjugated polymers have attracted great attention as candidate light-emitting materials for display application [1–5]. Fluorene and their derivatives have similar conjugated structures and can be applied as electro-active materials. The synthesis method and crystal parameters of diimines derived from fluorenone and phenylenediamine have been reported [6,7]. The diimines were synthesized by the p-toluenesulfonic acid-assisted Schiff base reaction between fluorenone and phenylenediamine.

Scanning tunneling microscopy (STM) and scanning tunneling spectroscopy (STS) have been used to investigate the charge transfer effect of molecule–substrate contact [8]. Molecule–substrate contact is a key to the molecular electronic devices, such as light-emitting medium and field-effect transistors [9]. The molecules of metal phthalocyanines and metalloporphyrins and their derivatives have been intensively studied [8,10–14]. Using double-end functional molecule, such as alkanedithiol to form the self-assembled monolayer on Au(111) is a useful approach to fabricate multilayer nanostructures, in which Deng and Bai built an Ag-dithiol–Au multilayer structure by adsorbing silver ions from solution onto the surface of self-assembled monolayer (SAM) of dithiols on Au(111) [15]. Orbital-mediated tunneling (OMT) spectra are helpful for investigating the affinity levels and the ionization levels. However, the agreement between the observed energies and those from ultraviolet photoelectron spectroscopy (UPS) and

electrochemistry does not provide the information that whether the spectra have identical results at any tip–substrate separations. The possibility that change the distance between the tip and monolayer might change the OMT peak positions was proposed by theoretical [16–20] and experimental [21–28] studies. Distance dependent current–voltage curves obtained from chemical vapor deposit (CVD) diamond films have been interpreted by tip field induced band bending at the semiconductor [23]. Scanning tunneling spectroscopic studies have been performed on the Si-terminated 6H-SiC(0001)(3 × 3) surface [25]. The spectra exhibit distinct bands of empty and filled states at large tip–substrate distances. But the STS spectra became completely featureless in the range of small tip–substrate distance. A model for the tunneling process had been proposed to explain the distance dependence [16,19]. In their model, the local field at molecule differs significantly with the applied sample bias. Deng and Hipps studied the tip–substrate distance dependence in the STM-based OMTS of NiTPP deposited on Au(111) [28]. They gave the result that difference of tip–substrate distance over several angstroms had produced no measurable changes in orbital energy splitting. However, an undetermined small but persistent shift of all OMTS was also observed in their studies. Tunneling conductance spectra were measured using STM tip and substrate as the electrodes, respectively [29]. The location of equilibrium Fermi energy and the spatial profile of the electrostatic potential under an applied bias have been thought as important parameters that influence the tunneling conductance spectra.

In this study, we report an experimental study on the N,N'-bis(9H-fluoren-9-ylidene)benzene-1,4-diamine thin films deposited on substrate. The thin films were characterized by

* Corresponding author. Tel.: +86 020 22236708; fax: +86 020 22236706.
E-mail address: wldeng@scut.edu.cn (W. Deng).

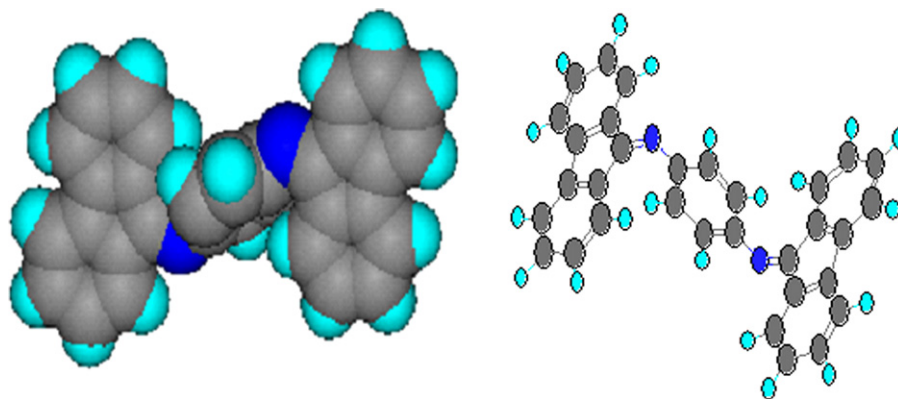


Fig. 1. The space-filling model and ball-stick mode of BFBD molecule. The color code used is as follows: carbon is gray, hydrogen is green and nitrogen is blue (For interpretation of the references to color in this figure legend, the reader is referred to the web version of the article.).

contact angle, X-ray photoelectron spectroscopy and tunneling conductance spectroscopy. Due to the importance of electrode distances in electron tunneling and molecular electronics, the relations between electrode–electrode distances and tunneling conductance were investigated. The tunneling current and conductance were measured to find the essential of tunneling behavior through molecular layers. Our results indicate that the tunneling conductance spectrum is dependent on the electric field between the tip and substrate. The electric field, changed by adjusting the setpoint current prior to spectral

measurement, plays an important role in the tunneling behavior.

2. Experimental

2.1. Materials

N,N'-bis (9*H*-fluoren-9-ylidene)benzene-1,4-diamine [$C_{22}H_{20}N_2$, BFBD molecule] was synthesized via the acetic acid-assisted Schiff base reaction between 9-fluorenone and *p*-phenylenediamine. The synthesized compound was purified by means of re-crystal in CH_2Cl_2 , which produced red rod crystals. The synthesized product and its structure were confirmed by melting point measurement, mass

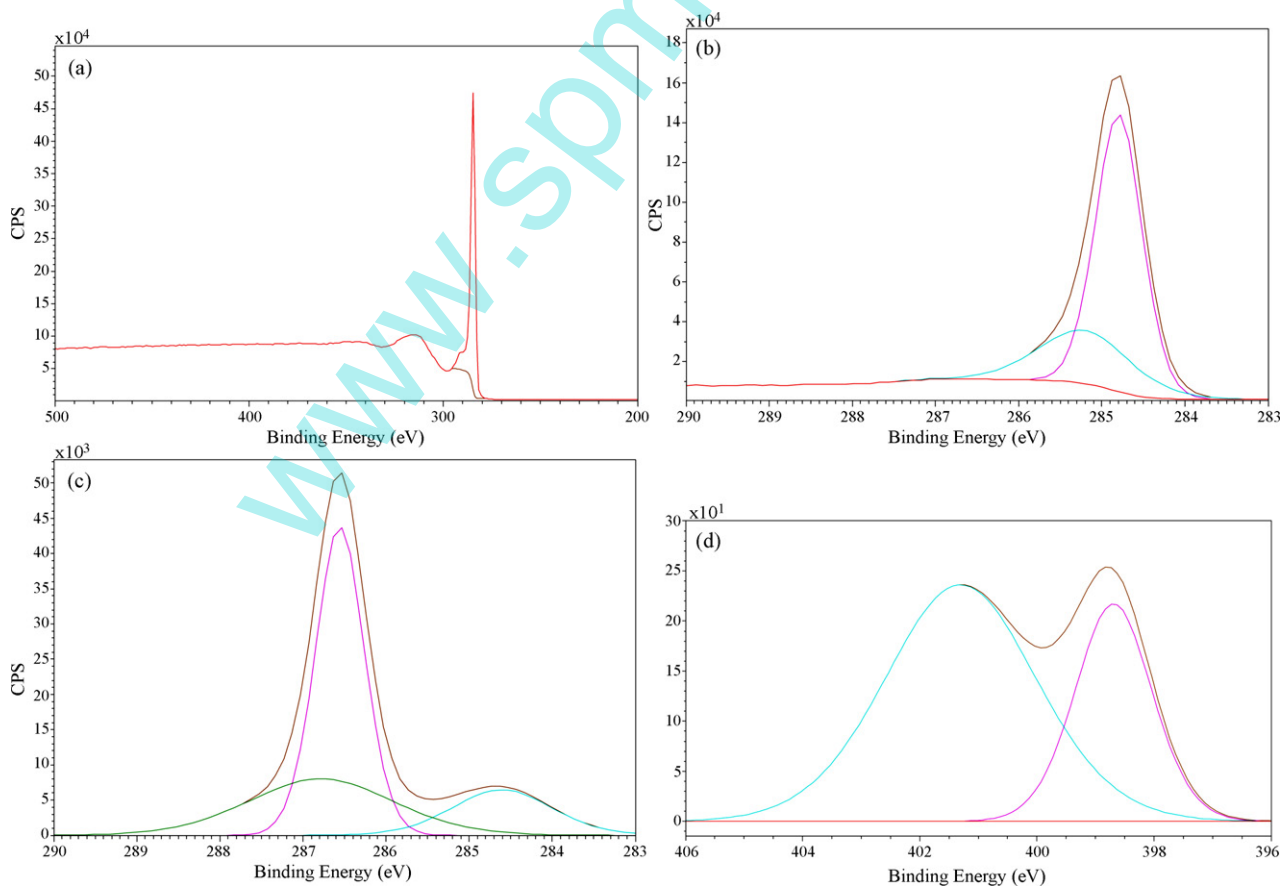


Fig. 2. (a) X-ray photoelectron spectroscopy of substrate, (b) high-resolution region of the XPS C1s for substrate, (c) high-resolution region of the XPS C1s for sample layers and (d) high-resolution region of the XPS N1s for sample layers.

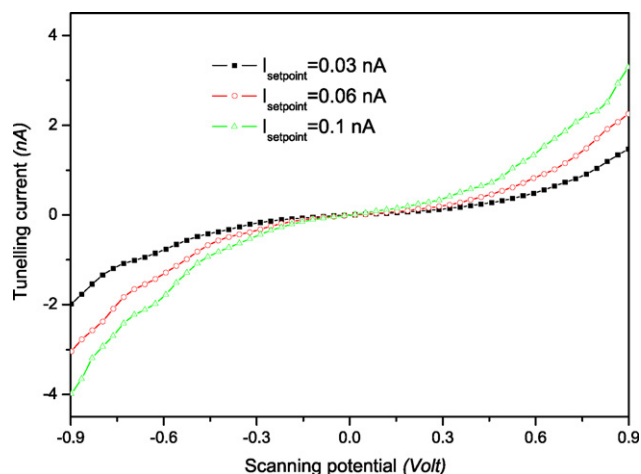


Fig. 3. The tunneling current curves as a function of scanning potential at different tip-substrate separations.

spectrum (MS), infrared spectrum (IR), Raman spectrum, Magnetic Resonance (MR) analysis, and X-ray diffraction (XRD) analysis. The results will be published elsewhere. The space-filling model and ball-stick model of the compound are shown in Fig. 1. BFBD thin films were deposited from solution onto highly oriented pyrolytic graphite for further studies. The solution of BFBD was prepared in dichloromethane with a concentration of $2 \times 10^{-3} \text{ mol l}^{-1}$. Solution of $5 \mu\text{l}$ were placed on graphite. After the solvent was evaporated, the sample was prepared. Highly oriented pyrolytic graphite (HOPG) was purchased from SPI Structure Probe Inc. (West Chester, PA, USA).

2.2. Contact angle measurements

Water contact angle measurement was performed on a contact angle system OCA 40 (Data Physics Instruments, Germany) using the sessile drop method at room temperature. Water drops of $2 \mu\text{l}$ were contacted with samples and the contact angles were recorded using photographic images. All

the contact angles here are the average values of five independent measurements.

2.3. X-ray photoelectron spectroscopy (XPS) data acquisition

X-ray photoelectron spectroscopy measurements were performed in a Kratos Axis Ultra DLD spectrometer with a focused monochromatic Al $K\alpha$ X-ray source ($h\nu = 1486.6 \text{ eV}$). The base pressure in the analysis chamber is about $1 \times 10^{-8} \text{ Torr}$. Spectra were recorded using pass energy of 160 eV at a resolution of 1 eV, while high-resolution spectra were acquired with pass energy of 20 eV at a resolution of 0.1 eV. All binding energies in X-ray photoelectron spectroscopy were internally referenced to C1s peak, which was assigned a value of 284.6 eV.

Tunneling conductance spectra Samples Preparation and Data Acquisition: Tunneling conductance spectra measurements were carried out with CSPM4000 scanning probe microscope system under ambient conditions. Tip was employed as an electrode which had been made mechanically with Pt/Ir (80:20) wire. The substrate was used as the other electrode. The uppermost layer of HOPG was peeled off immediately before use. A droplet of sample solution was applied on the fresh surface to form thin films. Spectroscopy was performed by measuring tunneling current as a function of bias voltage at fixed tip-substrate separation (feedback off). The method of measuring spectroscopy curve was reported [28]. The spectra data were acquired with a fixed tip-substrate separation determined by a selected bias voltage and tunneling current. The scanning potential was ramped from -1 to $+1 \text{ V}$. During this ramp, the spectroscopy curves were acquired at 512 points with a dwell time of about $200 \mu\text{s}$ per point. Then the bias and the setpoint were reset to re-establish the feedback loop. All the spectra were acquired at the temperature of about 298 K.

2.4. Computational detail

The density functional theory method with B3LYP on the basis of 6-31G (d) was employed to analyze the electron distribution. All computations were performed using the Gaussian03 package [30]. From these calculations, the characteristics of electron distribution and spatial orbital distributions were derived.

3. Results and discussion

The changes in water wettability of fresh substrate and the sample deposited on substrate were measured. The results showed

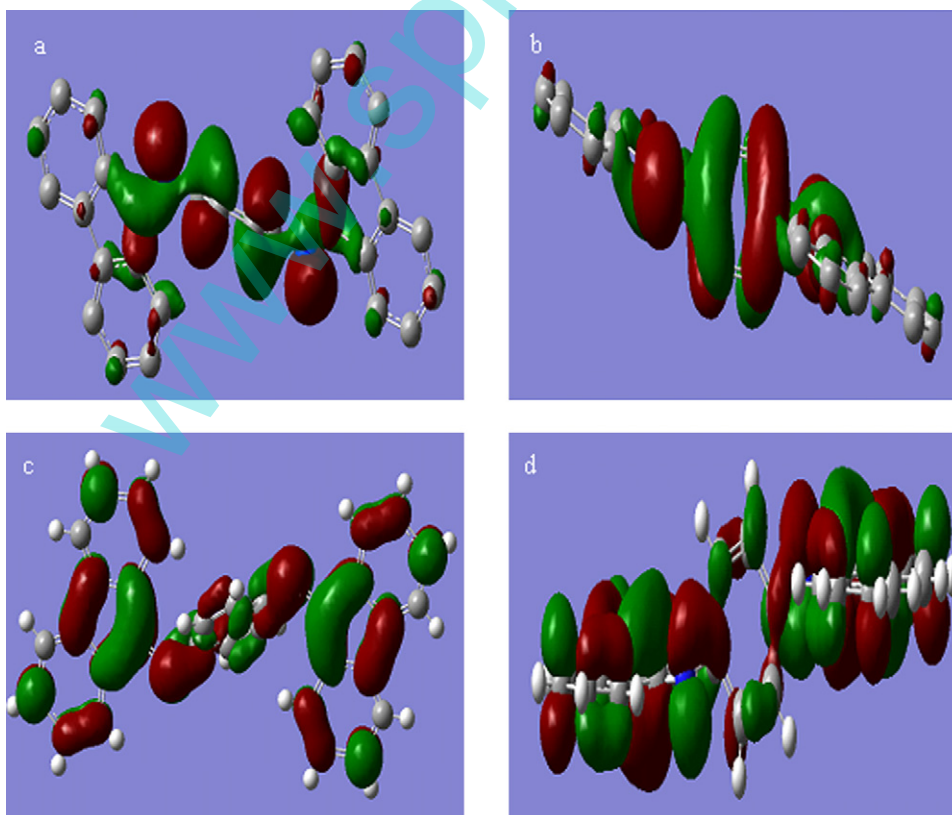


Fig. 4. Electron distribution. (a) Top view and (b) side view of the molecular HOMO. (c) Top view and (d) side view of the molecular LUMO.

that the water contact angel of pure substrate is about 50°. After deposition of sample on substrate, the contact angle approached 90°. The difference results from the change of densely packed array structure on substrate surface after deposition of sample [31].

Fig. 2 shows X-ray photoelectron spectroscopy patterns of substrate (Fig. 2a and b) and the sample deposited on substrate (Fig. 2c and d). Fig. 2c and d presents high-resolution region of the XPS spectra of C1s and N1s of sample, respectively. The nitrogen 1s peak can be decomposed into two peaks at 398.69 and 401.3 eV. The two peaks correspond to the pyridine- and graphitic-type bonding [32]. So the nitrogen atom cannot result from the atmosphere during handing the sample in air. The C1s spectrum of substrate shows a peak between 284 and 287 eV which can be decomposed into two bands at 284.79 and 285.2 eV (Fig. 2b). However, the C1s spectrum of sample deposited on substrate shows a peak which can be decomposed into three bands at 284.61, 286.56 and 286.79 eV, respectively. The chemical shift of C1s spectrum results from the deposition of sample on substrate.

Fig. 3 presents the tunneling current curves as a function of scanning potentials obtained at different tip–substrate separations. The tip–substrate distance was changed by resetting the setpoint prior to measuring the current curves. The form of current curve as a function of potential is similar. However, obvious difference can be founded in current curves. The current increases with setpoint at the same scanning potential.

In order to interpret the difference of current curve with various tip–substrate separations and find the electron transport mechanism through BFBD molecule, the special terms will be used. The scanning potential refers to the ramp voltage at fixed tip–substrate distance. The maximum of the electric field refers to the maximum value of electric field at fixed tip–substrate distance when scanning potential applied to the sample. The tip–substrate separations mean the electrode–electrode distances in tunneling conductance spectra measurement.

The following discussion is assumed that positive bias is applied to the substrate. In the first step, we analyzed the electron distribution of the compound, as it is of major impact on the electron transport properties. Fig. 4 shows the spatial electron distribution of HOMO and LUMO on the basis of quantum chemistry calculation. The electron configuration of carbon is $1s^2 2s^2 2p_x^1 2p_y^1$, and that of nitrogen is $1s^2 2s^2 2p_x^1 2p_y^1 2p_z^1$. The formation of BFBD molecule causes the element of nitrogen has lone pair. The lone pair, confined in nitrogen atom, contributes to the HOMO. When the positive bias is applied to the substrate, the BFBD molecule is exposed to the electric field. Under the action of Coulomb force in electric field, the lone pair of nitrogen atom can be transported through fluorene plane to the substrate.

The spatial orbits have evident difference between HOMO and LUMO of active layers, showed in Fig. 4. Suppose that positive bias is applied to the measure system. Electrons of nitrogen atom deviate from their own position under the action of electric field. In this case, the BFBD molecule is polarized and the harmonic oscillator is formed. According to the quantum mechanics theory of harmonic oscillator [33], the possible energy eigen-values of Hamiltonian can be described as. This means that the electronic energy at some special scanning voltage can come into resonance with the harmonic oscillator energy level. So several peaks at special potential can be observed going with the increase of scanning potential. Under the case of low electric field, the tip–substrate separation is so large that the change of electric field between the tip and substrate can be neglected. So the change of distance has little impact on the potential where the peak of differential current curve occurs. These results are consistent with the previous report [28].

In order to understand electron transport, it is necessary to analyze the tunneling conductance behavior. Some special potential

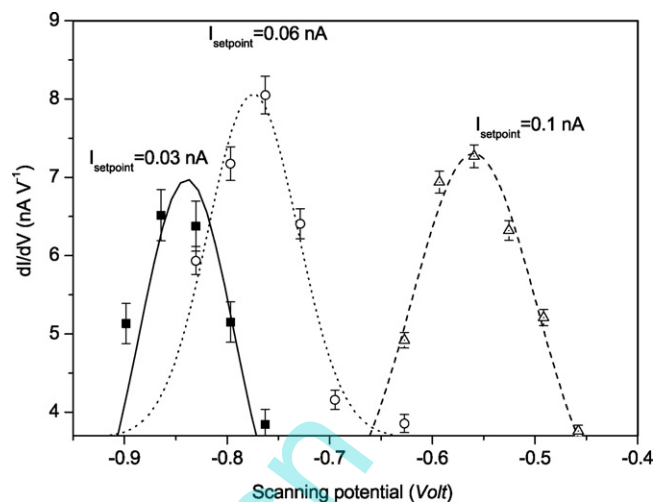


Fig. 5. The tunneling conductance peaks dependence on scanning potential. Each error bar represents one standard deviation from the mean of at least five experiments.

can be found and the peaks of tunneling conductance curve occur at these voltage. Fig. 5 shows the tunneling conductance spectra of BFBD thin films at special scanning potential region. Due to the similarity between positive potential and negative potential, the negative potential is selected to analyze the tunneling conductance. The potential data in different tip–substrate separations where the tunneling conductance reaches the maximum were listed in Table 1. With the decrease of tip–substrate separation, the maximum of the electric field between the tip and substrate is increased exponentially. However, the positions of the peak shift toward lower bias with the shrinkage of tip–substrate separation, the trend is shown in Figs. 5 and 6. That is because the distance is so small that the trivial shrinkage of tip–substrate can lead to striking increase of electric field that cannot be neglected. The effect of distance dependence leads to the decrease of the peak potential with the shrinkage of tip–substrate distance.

The classical theory of electron transfer can describe the process of electron transfer and the electron transfer rate is given by the golden rule-based expression under the Condon approximation [34]:

$$k_{\text{et}} = \frac{2\pi}{\hbar} |V_{\text{DA}}|^2 \text{FC} \quad (1)$$

$$\text{FC} = \sum_{\nu_D} \sum_{\nu_A} P_{\text{th}}(\varepsilon_D(\nu_D)) |\langle \nu_D | \nu_A \rangle|^2 \delta(\varepsilon_A(\nu_A) - \varepsilon_D(\nu_D) + E_{\text{AD}}) \quad (2)$$

where V_{DA} is the coupling between the donor (D) and acceptor (A) electronic states and FC is the thermally averaged and Frank–Condon weighted density of nuclear states. In equation (2), ν_D and ν_A denote donor and acceptor nuclear states, P is the Boltzmann distribution over donor states, $\varepsilon_D(\nu_D)$ and $\varepsilon_A(\nu_A)$ are nuclear energies above the corresponding electronic origins, and E_{AD} is the electronic energy gap between the donor and acceptor states. Considered the measurement process of tunneling conductance

Table 1

The potential data of N,N'-bis(9H-fluorene-9-ylidene)benzene-1,4-diamine in different tip–substrate separations where the tunneling conductance reach maximum. The maximum deviation from the mean of at least five experiments is listed.

Setpoint (nA)	Potential of peak (V)	Deviation	Potential of peak (V)	Deviation
0.03	-0.86441	3.84%	0.83051	3.99%
0.06	-0.76271	3.69%	0.79661	3.53%
0.1	-0.55932	5.01%	0.52542	5.32%

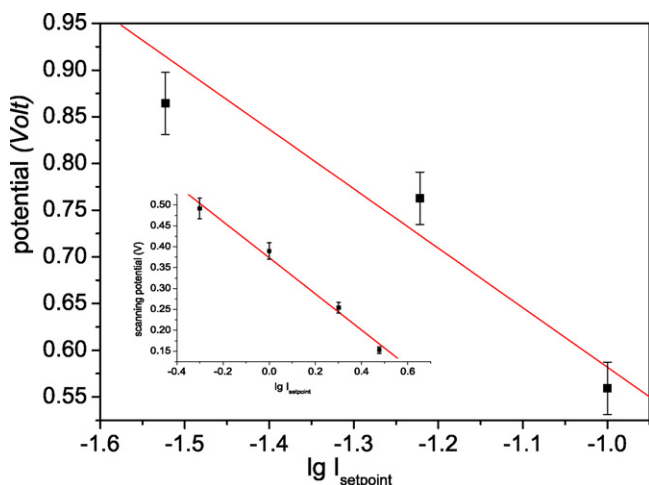


Fig. 6. The potential dependence on the tip–substrate distance where the tunneling conductance reach maximum. The tip–substrate distance was regulated by setpoint current. The inset is the minimal potential dependence on the tip–substrate distance where the tunneling current reaches 5 nA. The standard deviation is elucidated with error bars.

spectra, the electron transfer rate is found to decrease exponentially with the donor–acceptor distance,

$$k_{et} = k_0 e^{-\beta d} \quad (3)$$

where β is the range parameter that characterizes the distance dependence of the electron transfer rate, d is the distance between the tip and substrate and k_0 is a constant unrelated to d . Tunneling current is proportionate to the electron transfer rate k_{et} and can be described as

$$I_{set} = \alpha k_{et} = \alpha k_0 e^{-\beta d} \quad (4)$$

where I_{set} is the tunneling current that determines the tip–substrate distance, α is a constant factor that determines the relation between tunneling currents and tip–substrate distances.

The electric field between the tip and substrate is related to both scanning potential and electrode–electrode distance, can be depicted as

$$E = \gamma \frac{V}{d} \quad (5)$$

Eqs. (4) and (5) result in

$$V = \frac{E}{\gamma} d = \frac{E \lg(\alpha k_0)}{\gamma \beta \lg e} - \frac{E}{\gamma \beta \lg e} \lg I_{set} \quad (6)$$

where V is the potential that caused the electric field E under the special tip–substrate distance. γ and e are constant factor.

Due to the transmission function is increasing exponentially with the decrease of the tip–substrate distances [34] and the exponential dependence is also found in experiment [35], the Landauer theory can give uniform results.

Fig. 6 shows the potential dependence on the tip–substrate distance where the tunneling conductance reaches the maximum. The tip–substrate distance was regulated by the setpoint current. The potential decreases with the increase of setpoint current that leads to the shrinkage of tip–substrate separation. The inset is the minimal potential where the tunneling current reaches 5 nA at different tip–substrate distances. The slope of line in **Fig. 6** reveals that the special electric field is constant, which is depicted in Eq. (6). The above result is assumed the positive potential applied to the sample, the same conclusion can be drawn when the potential is negative.

4. Conclusion

The derivative of fluorene, which is called N,N'-bis(9H-fluorenyl-9-ylidene)benzene-1,4-diamine, was synthesized via the acetic acid-assisted Schiff base reaction between 9-fluorenone and p-phenylenediamine. The thin films of the diamine were fabricated and systemically researched, such as X-ray photoelectron spectroscopy and so on, were presented. From above discussions, the conclusion can be drawn that the potentials, which lead to the tunneling conductance peaks, depend not only on the scanning potential, but also on the electric field applied to the thin films. The electric field dependence is manifested significantly. The results of this study contribute to the properties and potential application of this composite material.

Acknowledgments

This work was supported financially by the State Key Development Program for Basic Research of China (2009CB930604) and the Natural Science Foundation of Guangdong Province, China (8151064101000111).

References

- [1] J.H. Bourroughes, D.D.C. Bradley, A.R. Brown, R.N. Marks, K. Mackey, R.H. Friend, P.L. Burns, A.B. Holmes, *Nature* 347 (1990) 539.
- [2] A. Kraft, A.C. Grimsdale, A.B. Holmes, *Angew. Chem. Int. Ed.* 37 (1998) 402.
- [3] S.W. Ko, B.J. Jung, T. Ahn, H.K. Shim, *Macromolecules* 35 (2002) 6217.
- [4] Q. Pei, Y. Yang, *J. Am. Chem. Soc.* 118 (1996) 7416.
- [5] M. Ranger, D. Rondeau, M. Leclerc, *Macromolecules* 30 (1997) 7686.
- [6] N.M. Glagovich, M.R. Elizabeth, G. Crundwell, J.B. Updegraff, Z. Matthias, A.D. Hunter, *Acta Cryst. E61* (2005) o1251.
- [7] D.K. Benya, J.F. Freitas, G. Crundwell, N.M. Glagovich, *Acta Cryst. E62* (2006) o1639.
- [8] S.B. Lei, K. Deng, D.L. Yang, Q.D. Zeng, C. Wang, *J. Phys. Chem. B* 110 (2006) 1256.
- [9] S.R. Forrest, *Chem. Rev.* 97 (1997) 1793.
- [10] T.A. Jung, R.R. Schlittler, J.K. Gimzewski, H. Tang, C. Joachim, *Science* 271 (1996) 181.
- [11] J.K. Gimzewski, T.A. Jung, M.T. Cuberes, R.R. Schlittler, *Surf. Sci.* 386 (1997) 101.
- [12] K.W. Hipps, D.E. Barlow, U. Mazur, *J. Phys. Chem. B* 104 (2000) 2444.
- [13] L. Scudiero, D.E. Barlow, U. Mazur, K.W. Hipps, *J. Am. Chem. Soc.* 123 (2001) 4073.
- [14] W. Deng, D. Fujita, T. Ohgi, S. Yokoyama, K. Kamikado, S. Mashiko, *J. Chem. Phys.* 117 (2002) 4995.
- [15] W. Deng, L. Yang, D. Fujita, H. Nejo, C. Bai, *Appl. Phys. A* 71 (2000) 639.
- [16] W. Schmickler, *J. Electroanal. Chem.* 296 (1990) 283.
- [17] A.I. Oniplo, K.F. Berggren, Y.O. Klymenko, L.I. Malysheva, J.J.W.M. Rosink, L.J. Geerligs, E. van der Drift, S. Radelaar, *Phys. Rev. B* 61 (2000) 11118.
- [18] M. Plihal, J.W. Gadzuk, *Phys. Rev. B* 63 (2001) 085401.
- [19] H. Sumi, *J. Phys. Chem. B* 102 (1998) 1833.
- [20] J. Zhang, Q. Chi, A.M. Kuznetsov, A. Hansen, H. Wackerbarth, H.E. Christensen, J. Andersen, J. Ulstrup, *J. Phys. Chem. B* 106 (2002) 1131.
- [21] E.P. Bakkers, Z. Hens, L.P. Kouwenhoven, L. Gurevich, D. Vanmaekelbergh, *Nanotechnology* 13 (2002) 258.
- [22] D. Katz, O. Millo, S. Kan, U. Banin, *Appl. Phys. Lett.* 79 (2001) 117.
- [23] S.R. Snyder, H.S. White, *J. Electro. Chem.* 394 (1995) 177.
- [24] M. Cannars, M. Nesladek, K. Haenen, D.L. Schepper, L.M. Stals, V.C. Haendonck, *Diamond Relat. Mater.* 11 (2002) 212.
- [25] V. Gasparov, M. Riehl-Chudoba, M. Schroter, W. Richter, *Europhys. Lett.* 51 (2000) 527.
- [26] W. Han, E.N. Durantini, T.A. Moore, D. Gust, P. Rez, G. Letherman, G. Seely, N. Tao, S.M. Lindsay, *J. Phys. Chem. B* 101 (1997) 10719.
- [27] A.D. Muller, F. Muller, M. Hietschold, *Appl. Phys. Lett.* 74 (1999) 2963.
- [28] W. Deng, K.W. Hipps, *J. Phys. Chem. B* 107 (2003) 10736.
- [29] W. Tian, S. Datta, S. Hong, R. Reifenberger, J.I. Henderson, C.P. Kubiak, *J. Chem. Phys.* 109 (1998) 2874.
- [30] M.J. Frisch, G.W. Trucks, H.B. Schlegel, G.E. Scuseria, M.A. Robb, J.R. Cheeseman, J.A. Montgomery Jr., T. Vreven, K.N. Kudin, J.C. Burant, J.M. Millam, S.S. Iyengar, J. Tomasi, V. Barone, B. Mennucci, M. Cossi, G. Scalmani, N. Rega, G.A. Petersson, H. Nakatsuji, M. Hada, M. Ehara, K. Toyota, R. Fukuda, J. Hasegawa, M. Ishida, T. Nakajima, Y. Honda, O. Kitao, H. Nakai, M. Klene, X. Li, J.E. Knox, H.P. Hratchian, J.B. Cross, C. Adamo, J. Jaramillo, R. Gomperts, R.E. Stratmann, O. Yazyev, A.J. Austin, R. Cammi, C. Pomelli, J.W. Ochterski, P.Y. Ayala, K. Morokuma, G.A. Voth, P. Salvador, J.J. Dannenberg, V.G. Zakrzewski, S. Dapprich, A.D. Daniels, M.C. Strain, O. Farkas, D.K. Malick, A.D. Rabuck, K. Raghavachari, J.B. Foresman, J.V. Ortiz, Q. Cui, A.G. Baboul, S. Clifford, J. Cioslowski, B.B. Stefanov, G. Liu, A. Liashenko, P. Piskorz, I. Komaromi, R.L. Martin, D.J. Fox, T. Keith, M.A. Al-Laham, C.Y. Peng, A. Nanayakkara, M. Challacombe, P.M.W. Gill, B. Johnson, W. Chen,

- M.W. Wong, C. Gonzalez, J.A. Pople, The hybrid DFT functional is chosen to be B3LYP, namely, Becke's 3 parameter exchange functional plus Lee-Yang-Parr correlation functional, in: Gaussian 03, Revision B. 01, Gaussian, Inc, Pittsburgh PA, 2003.
- [31] X. Miao, A. Gao, S. Hiroto, H. Shinokubo, A. Osuka, H. Xin, W. Deng, Surf. Interf. Anal. 41 (2009) 225.
- [32] J. Liu, S. Webster, D.L. Carroll, Appl. Phys. Lett. 88 (2006) 213119.
- [33] P.A.M. Diarc, The Principles of Quantum Mechanics, Oxford University Press, London, 1958.
- [34] A. Nitzan, Annu. Rev. Phys. Chem. 52 (2001) 681.
- [35] D.J. Wold, R. Haag, M.A. Rampi, C.D. Frisbie, J. Phys. Chem. B 106 (2002) 2813.

www.spm.com.cn